Gecko-Inspired Climbing Behaviors on Vertical and Overhanging Surfaces

Daniel Santos, Barrett Heyneman, Sangbae Kim, Noe Esparza, and Mark R. Cutkosky

Center for Design Research

Stanford University

Stanford, CA 94305-2232, USA

contact: dsantos@stanford.edu

Abstract— The adhesive and frictional properties of dry adhesive materials can be described by a three-dimensional limit surface in the space of normal and tangential contact forces at the feet. We present the empirically derived limit surface for directional adhesive pads and illustrate its application to controlling the forces at the feet of a robot climbing on arbitrary slopes, including overhanging surfaces. For the directional adhesive patches that we have developed, the limit surface is convex, which permits efficient computation of the desired internal and external forces among the feet to maximize a safety margin with respect to disturbance forces on the robot. The limit surface also intersects the origin in force space, which enables efficient climbing without wasting energy in attaching and detaching the feet. These insights are applied to an experimental climbing platform demonstrating the proper use of directional adhesion and mimicking the climbing behavior seen in geckos.

I. Introduction

As progress continues in legged robotics, research has begun to focus on developing robust climbers. Various robots have been developed that climb flat vertical surfaces using suction [16], [17], [21], magnets [6], [23], and arrays of small spines [1], [20] to attach their feet to the surface. More recently, robots have been developed that utilize adhesive materials for climbing smooth surfaces such as glass [7], [15], [18].

Researchers have also begun to examine the adhesive structures of the gecko lizard in detail, inspired by the gecko's remarkable speed and ability to climb a wide variety of surfaces. The gecko employs a sophisticated hierarchical adhesive system consisting of lamellae, setae, and spatulae [4], [5] that conform intimately to both smooth and rough surfaces, allowing van der Waals forces to provide sufficient adhesion for climbing. In addition, the adhesive structures are angled and curved, which gives gecko adhesion the important property of directionality [2]. When the adhesive structures are pulled tangentially to the climbing surface in one direction, the amount of adhesion at the contact linearly increases with the amount of shear; when shear forces are applied in the opposite direction, only friction is observed. The directional property of gecko adhesion has been described by an empirical model termed *frictional adhesion* [3].

In previous work, the authors reported on a synthetic adhesive material that mimics the directional property of gecko adhesion [19] and on the design and operation of a legged
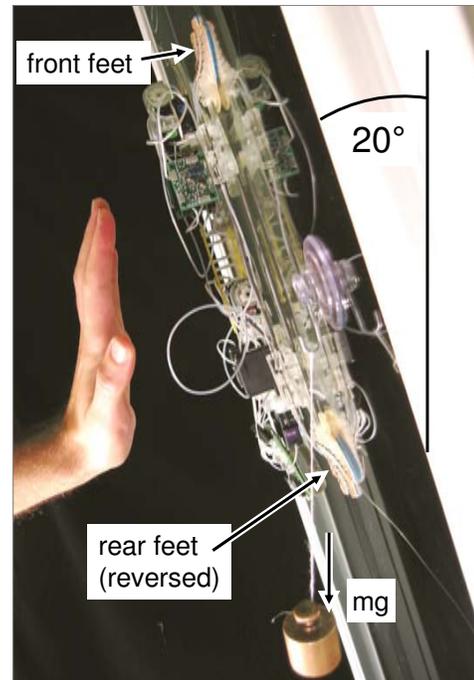

Fig. 1. StickyBot ($\sim$450g) shown clinging to an overhanging (20° beyond vertical) surface, with rear feet reversed and with $\sim$6N internal force applied between front and rear feet in the fore-aft direction (3N on both left and and right sides). (Weight hanging from suction cup in foreground shows gravity direction.)

robot that utilizes this material to climb smooth vertical surfaces [15]. In the present paper, we extend this work to develop a three-dimensional limit surface that describes combinations of normal, tangential and lateral forces that a directional adhesive contact can sustain without failing due to slippage or detachment. The 3D force limit surfaces for individual contact patches are then combined, using convex addition, to obtain an overall limit surface for an entire foot. We use the limit surfaces as constraints in a force analysis to prescribe optimal foot orientations and internal forces to apply at the feet of a climbing robot, to maximize its ability to resist arbitrary disturbance forces on sloped and overhanging surfaces. We demonstrate the application of this analysis to StickyBot (Fig. 1) allowing it to cling to overhanging surfaces. We conclude with a discussion of future extensions of the work.
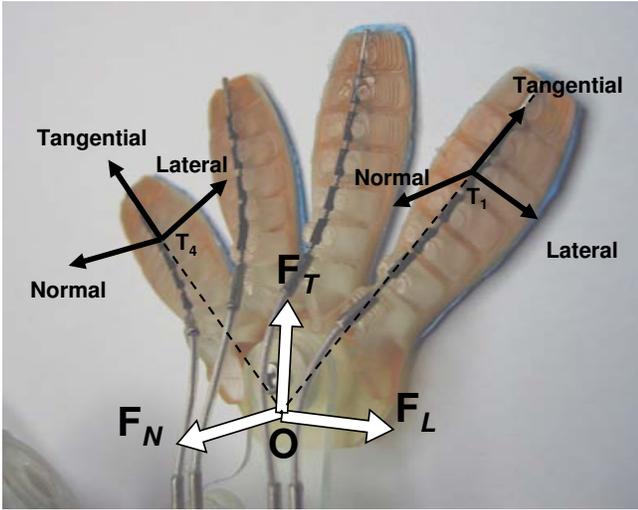
Fig. 2. A StickyBot foot has four toes, each of which has a $4\mathrm{cm}^2$ patch of a synthetic adhesive termed Directional Polymer Stalks (DPS). The preferred loading direction for each patch is along the tangential axis. The tangential, lateral and normal axes form a right-handed coordinate system for each patch, as shown. The four patches combine to produce a resultant lateral, tangential and normal force for the entire foot.

Fig. 3. Pull-off force in the normal direction as a function of preload. The pull-off force begins to saturate at preload forces above $\sim$1N, corresponding to preload depths larger than $700\mu\mathrm{m}$.

II. THREE DIMENSIONAL ADHESION LIMIT SURFACE

Figure 2 shows one foot of StickyBot with four toes, each of which is equipped with a synthetic adhesive patch termed Directional Polymer Stalks (DPS) [19]. Because of the angled nature of the stalks in the DPS patches, they exhibit directional adhesion similar to that observed in the gecko [3], [19].

To obtain a more complete, three-dimensional characterization of the friction and adhesion, new experiments were performed that included the effects of loading in all three directions: normal, tangential and lateral (see Fig. 2). A 3-axis linear stage was used to apply motions to DPS patches, bringing them into and out of contact with a glass substrate. The motion stage (Velmex, MAXY4009W2-S4 and MA2506B-S2.5) has a positioning resolution of $\pm10\mu\mathrm{m}$ in the lateral and tangential directions and $\pm1\mu\mathrm{m}$ in the normal direction. The flat glass substrate is mounted on a 6-axis force/torque sensor (ATI Industrial Automation, Gamma Transducer SI-32-2.5), which is in turn mounted on a manual 2-axis tilt stage (Newport, 30 Series Tilt Platform) used for aligning the sample to the substrate.

Experiments consisted of first preloading patches along an approach trajectory to a desired depth in the normal direction. The patches were then pulled away from the substrate and the pull-off and/or sliding forces were measured in the lateral, tangential, and normal directions. Both the preload trajectory angle and the preload depth were varied in order to determine their effect on normal pull-off forces.

For the initial tests, pull-off vectors were constrained to the tangential-normal plane (Fig. 2) and speed was held constant at $1\mathrm{mm/s}$. A preload approach angle of $45°$ was empirically found to produce the largest pull-off forces for any given preload. Pull-off forces quickly drop as the approach becomes shallower (more dragging) or steeper
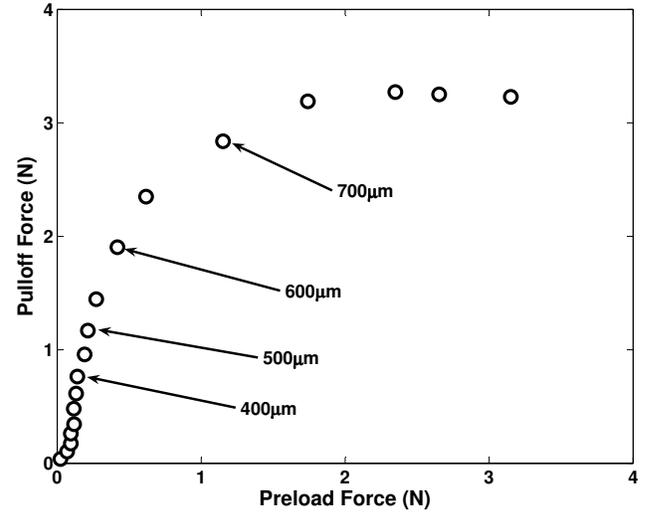
(normal approach vector). In these tests, the preload force was indirectly controlled by specifying the approach depth in the normal direction. Figure 3 shows the variation of normal pull-off force with preload. Pull-off force increases with preload up to a depth of $\sim700\mu\mathrm{m}$, after which the force begins to saturate.

Further testing of the DPS consisted of using pull-off directions spanning the three-dimensional lateral, tangential and normal space. These motions resulted in various combinations of positive and negative lateral, tangential, and normal forces, which were measured with the 6-axis load cell. The preload approach angle was fixed at $45°$ and preload depths fixed at $500\mu\mathrm{m}$ and $700\mu\mathrm{m}$ based on initial experiments. The larger preload value gives higher adhesion; the smaller is more consistent with the normal forces that the actuators on StickyBot exert during climbing.

Results from these experiments are used to construct a three-dimensional limit surface for a contact patch. Approximately 300 different exit paths are generated, each of which is repeated 3 times to check for repeatability. The average standard deviation is approximately 0.04N. The entire test for characterizing an adhesive patch is automated and takes approximately 4 hours. Figures 4 and 5 show cross sections of this limit surface in the tangential-normal and lateral-normal planes, respectively. Fitting the parameters of the directional adhesion model from [3] to the case of $700\mu\mathrm{m}$ results in an estimated angle of $\alpha^* = 25°$ describing the relationship between maximum adhesion and tangential force, a coefficient of friction of $\mu = 0.75$ for positive normal forces, and a limiting value of $F_{max} = 7N$ in the tangential direction. This limiting force is established by the ultimate saturation and sliding failure of the DPS as shown in Fig. 4.

In the lateral-normal plane, the DPS exhibit the symmetric behavior shown in Fig. 5. Both positive and negative lateral forces decrease the amount of adhesion present at the contact or increase the amount of compression required to avoid slip-
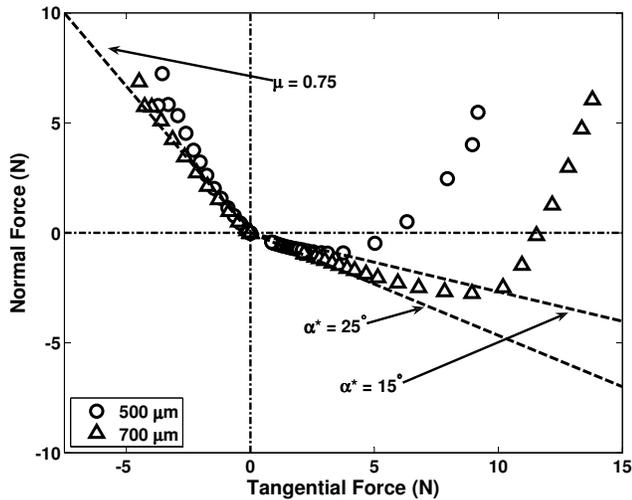
Fig. 4. Contact failure forces for the DPS plotted in the tangential-normal plane. Results are similar to the frictional adhesion model for the gecko, with adhesion initially increasing almost linearly with increasing tangential force. Beyond 7N of tangential force, the adhesion saturates and then diminishes as the directional stalks start to slide. Data are shown for preload depths of $500\mu m$ and $700\mu m$, illustrating the dependence of adhesion forces on preload.

Fig. 6. Contact failure forces for the DPS plotted in three dimensions. The limit surface has been constructed via linear interpolation of the experimental results. Only one half of the limit surface is shown for the sake of clarity since the results are roughly symmetrical about the tangential-normal plane (see Fig. 5). A plane at $F_N = 0$ has been included to highlight the shape and distinguish between adhesive and compressive portions of the surface.
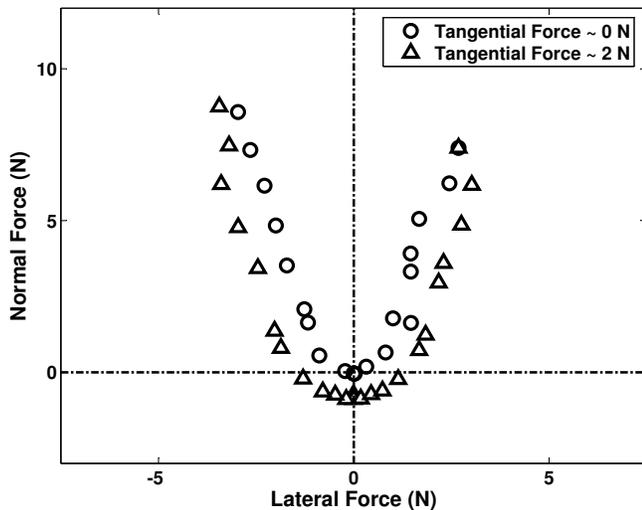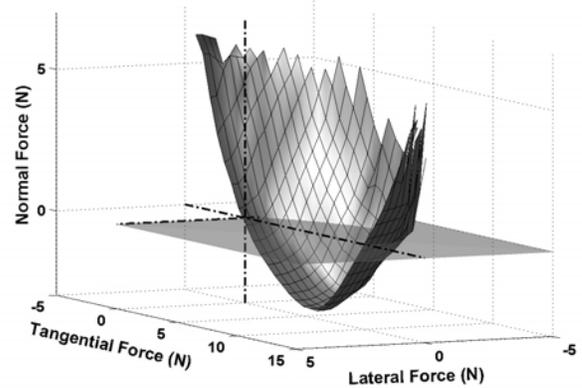

Fig. 5. Contact failure forces for the DPS plotted in the lateral-normal plane are symmetric and similar to previous isotropic adhesion models. When adhesion is initially present due to positive tangential forces, as shown in the lower curve, increasing the lateral force results in decreased adhesion.

ping. The behavior is similar to previous isotropic adhesion models [12], [13], [22], [24] including a simple early model proposed by Derjaguin [8], [9] in which the Coulomb friction cone is offset along the negative normal axis by an adhesion parameter.

Figure 6 shows the three-dimensional experimental limit surface plotted in the space of lateral, tangential and normal forces at a contact. Only one half of the surface is shown for clarity since the data are approximately symmetric about the tangential-normal plane (Fig. 5). Force vectors that are inside this surface can be sustained at the contact without producing slipping or pull-off. For positive normal forces,

failure will ultimately occur if the tangential force exceeds the friction limit or if the maximum tangential force, F_{max}, is reached. For negative normal forces, the available adhesion depends on the tangential and lateral forces. As seen in the Fig. 6, the limit surface is convex and asymmetric in the tangential-normal plane. It also intersects the origin in force space. As shown in the next sections, these properties are convenient when using the limit surface to prescribe forces and foot orientations for a climbing robot.

A. Producing a combined limit surface for several toes

The limit surface depicted in Fig. 6 is for a single toe. However, by resolving the forces to a common coordinate frame embedded in the foot (see Fig. 2) we can use convex, or Minkowski, addition [10], [11] to create an expanded limit surface for the entire foot. If each limit surface is described by a set of vectors, A and B, from the origin to the surface itself, then the Minkowski addition of two surfaces can be given as

$$A + B = \{a + b | a \in A, b \in B\}, \tag{1}$$

and likewise for more surfaces. In addition to being larger, due to the combined effects of four toes, the new limit surface has a wider profile in the lateral-normal plane due to the fact that the toes are not parallel but span an angle of $90°$ (see Fig. 2). Each toe's individual limit surface must first be described in a common coordinate system, resulting in four limit surfaces that are rotated with respect to one another, and are then added together through convex addiction.

B. Linearized LS Approximation

For the force analysis in the next section, the limit surface is approximated by a series of planes resulting in the following limits on the contact forces at a foot:
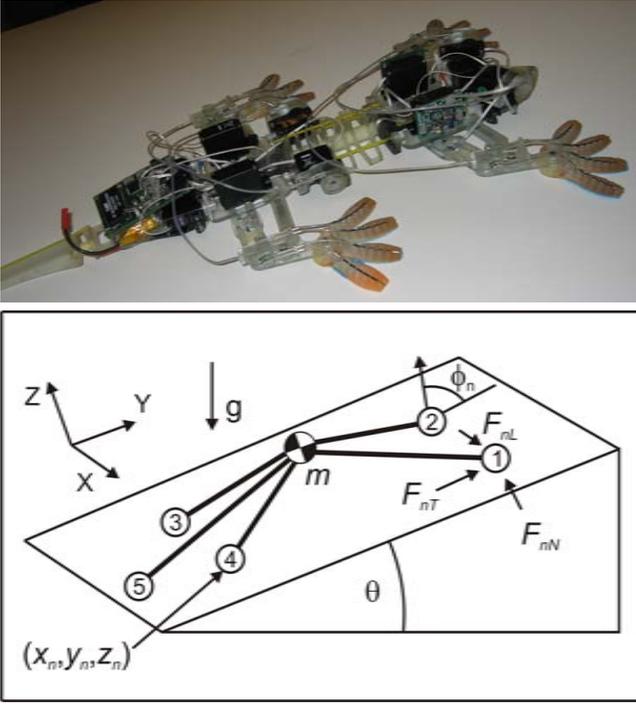
Fig. 7. Three-dimensional simplified model of StickyBot, represented as a center of mass, four foot contacts (n = 1-4) and one tail contact (5). Each foot has three associated contact forces (F_{nL}, F_{nT}, F_{nN}) and an orientation (ϕ_n) about the Z axis. The tail is comparatively frictionless and has only a normal force (F_{5N}). The climbing surface is inclined at an angle, θ.

$$
\begin{aligned}
-F_T &\leq \mu F_N \\
F_N &\geq -F_T \tan(\alpha^*) + \frac{1}{\mu}|F_L| \\
F_T &\leq F_{max},
\end{aligned}
\tag{2}
$$

where μ is the coefficient of friction in the lateral and negative tangential directions, α^* is the angle determining the adhesion limit in the positive tangential direction, and F_{max} is a limit on the maximum positive tangential force that can be applied. Fitting the above planes to a patch of the DPS results in an average error of 0.3N. Numerical values of μ, α^* and F_{max} for an entire foot of StickyBot are given in Table I. Eq. 2 is an extension of the frictional adhesion model [3] to include the effects of lateral forces.

III. FORCE ANALYSIS AND OPTIMIZATION

A simple three-dimensional model of a clinging robot can be used to illustrate the application of contact limit surfaces for specifying the forces and orientations of the feet. Figure 7 shows a climbing model represented by a center of mass, four foot contacts and a tail, resting on an inclined plane. The following analysis is similar to several analyses in the literature on dexterous manipulation, following the approach initially presented by Kerr and Roth [14], in which one solves for optimal contact forces, subject to the need to satisfy equilibrium and subject to force constraints at the contacts. The essential differences are that normal forces can now be negative as well as positive, and that the force constraints at each foot are now represented by Eq. 2 instead of a symmetric Coulomb friction cone or its pyramidal approximation.

There are six equations for static equilibrium and four foot contacts with three unknown forces each. It is assumed that moments about the lateral, tangential and normal axes at the feet are negligible because StickyBot has very rotationally compliant ankles. There is one additional unknown associated with the normal force at the comparatively frictionless tail. The result is an under-determined system, which can be written as

$$
\mathbf{WC} + \mathbf{F} = \mathbf{0},
\tag{3}
$$

where $\mathbf{C}$ is the 13×1 solution vector of contact forces, $\mathbf{F}$ is the vector of external forces and moments due to gravity, $\mathbf{W}$ is given by

$$
\mathbf{W} = \begin{bmatrix}
 & & & & 0 \\
\mathbf{I_3} & \mathbf{I_3} & \mathbf{I_3} & \mathbf{I_3} & 0 \\
 & & & & 1 \\
 & & & & y_5 \\
\hat{\mathbf{R}}_1 & \hat{\mathbf{R}}_2 & \hat{\mathbf{R}}_3 & \hat{\mathbf{R}}_4 & -x_5 \\
 & & & & 0
\end{bmatrix},
\tag{4}
$$

$\mathbf{I_3}$ is the 3×3 identity matrix, and $\hat{\mathbf{R}}_\mathbf{n}$ is the cross-product operator for each foot position vector.

The degrees-of-freedom in the system correspond to internal body forces that the feet and tail can exert without affecting equilibrium. For example, on a horizontal surface the front feet could apply forces in the Y (fore-aft) direction equal and opposite to those applied by the rear feet, resulting in no net tangential force.

Solutions to an under-determined system can always be found, but the contact forces at the feet and tail must also satisfy any contact requirements, such as friction and adhesion limits. If the contact constraints are linear, as in Eq. 2, they can be written generally as

$$
\mathbf{AC} \geq \mathbf{P},
\tag{5}
$$

where each row of the matrix inequality corresponds to a contact constraint specified in the contact models. For the tail, the constraint is just $F_N \geq 0$.

The optimization uses internal forces to move the contact forces at the feet and tail away from their respective limit surfaces, approximated by Eq. 2. By splitting the solution vector into its particular and homogeneous parts, the equilibrium and contact constraint equations can be combined as

$$
\mathbf{AN}\lambda \geq \mathbf{P} + \mathbf{AW}^\dagger \mathbf{F},
\tag{6}
$$

where $\mathbf{N}$ and $\mathbf{W}^\dagger$ are the nullspace and pseudo-inverse of $\mathbf{W}$, respectively, and λ is a vector of internal forces. Each row of Eq. 6 corresponds to a contact constraint. Stability can be maximized by choosing a λ that increases the distance by which each row in Eq. 6 is satisfied. Such an optimization

TABLE I

STICKYBOT PARAMETER VALUES FOR CLIMBING ANALYSIS

Parameter	Value
Model Parameters	
m	450g
$x_{1,4}, x_{2,3}$	8cm, -8cm
$y_{1,2}, y_{3,4}$	14cm, -14cm
x_5	0cm
y_5	-47cm
$z_{1,2,3,4,5}$	-2cm
$\phi_2(=-\phi_1)$	$0° : 90°$
$\phi_3(=-\phi_4)$	$0° : 180°$
θ	$0° : 180°$
Directional Adhesion Parameters	
μ	1.0
α^*	$15°$ to $25°$
F_{max}	3N

can be solved using standard linear programming methods, as used in [14].

The solution returns the optimal internal forces and the distance from violating any of the constraints. When formulated properly this distance corresponds to the stability margin of the system. It represents the maximum perturbation force, from any direction, that can be exerted at any contact without causing failure and it can be used to evaluate the relative safety of different kinematic configurations or climbing strategies. Note that this optimization produces a maximally safe set of foot forces, at the expense of high actuator forces or torques required to produce the internal forces between the feet. An alternative strategy, not considered here, would be to minimize actuator forces while maintaining a consistent margin of safety.

Because the limit surfaces are anisotropic, the orientation of the feet must also be specified. We assume that the orientation of each foot can range from $0°$ to $360°$ rotated about the contact normal (Z axis in Fig. 7). Given a set of foot orientations, the inequalities in Eq. 2 can be transformed to the body frame and written into the form of Eq. 5.

Figure 8 shows the effects of varying foot orientations on a vertical surface while keeping the internal forces between the feet adjusted for maximum stability, subject to constraints. To produce this plot, the body and contact parameters were taken from Table I, with $\alpha^* = 25°$ and F_{max} reduced from the ultimate $15N - 20N$ limit established by the adhesive patches to a conservative 3N in the tangential direction to account for actuator limits. The stability margin, in Newtons, is the maximum disturbance force that can be applied to any contact in any direction without causing any failures. We observe that there is a plateau of solutions with a stability of $\sim0.51N$ corresponding to a range of foot orientations. At one extreme, the rear feet are opposed ($\phi = 90°$) and the front legs bear the gravity load ($\phi = 0°$); at the other extreme the reverse is true, with the front feet pulling laterally inward and the rear feet supporting the gravity load.

For clinging to an inverted surface, where gravity is in the normal direction, a different strategy is optimal. In this case, the directional adhesion is generated entirely by internal forces and the tangential forces at the feet should all be in
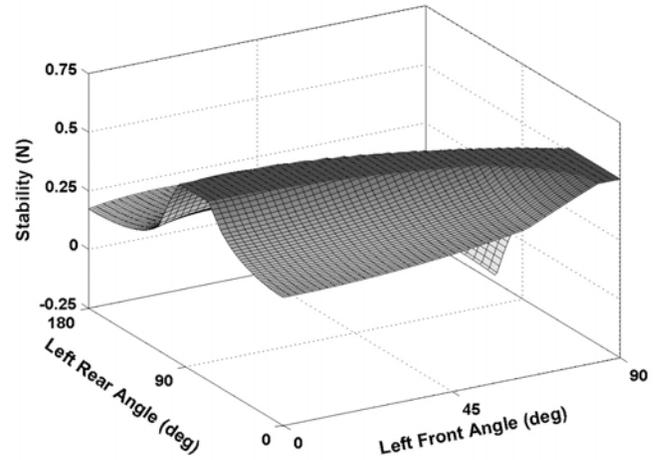

Fig. 8. Stability margin for different combinations of front and rear foot orientation angles on a vertical surface. A range of orientation angles exists that produce a maximum stability margin of $\sim0.51N$ with respect to disturbance forces in any direction.
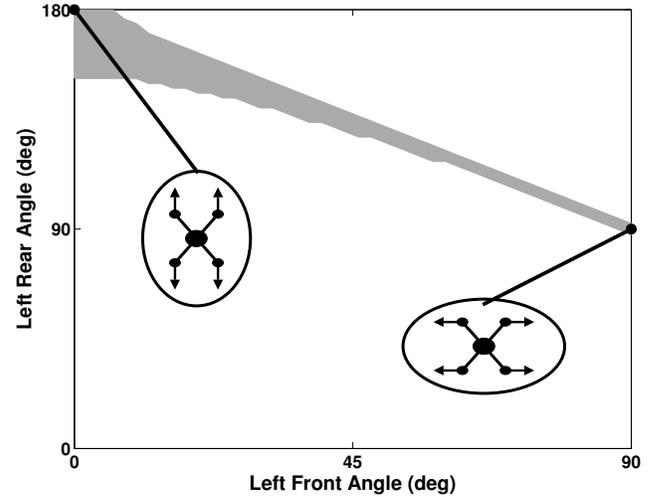

Fig. 9. Optimal foot orientations for clinging to an inverted surface. The gray band shows combinations of orientations that produce an optimal stability margin of $d \approx 0.1N$. In all cases, the feet are in opposition so that internal forces can produce the shear loading needed to maximize adhesion.

opposition (Fig. 9). We note that in this case, unlike surfaces with an inclination of $90°$ or lower, the tail is not helpful.

IV. APPLICATION TO THE CONTROL OF A CLIMBING ROBOT

The climbing strategies suggested by this analysis have been tested on StickyBot [15]. In the case of StickyBot, the foot orientations cannot be varied continuously; however the rear feet can be positioned manually to be aligned with the front feet ($\phi = 0°$ as shown in the photograph in Fig. 7) or reversed ($\phi = 180°$, as in the photograph in Fig. 1).

In addition, StickyBot is only able to control internal forces in the fore-aft (Y) direction and not in the lateral direction. Figure 10 shows the stability margin as a function of the inclination angle, with the rear feet either aligned or reversed, and with internal forces between the front and
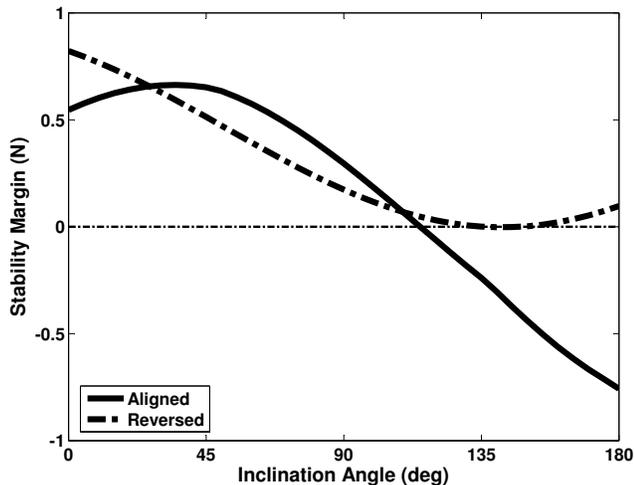
Fig. 10. Stability margin for StickyBot at different inclines with rear feet either aligned or reversed with respect to the front feet.
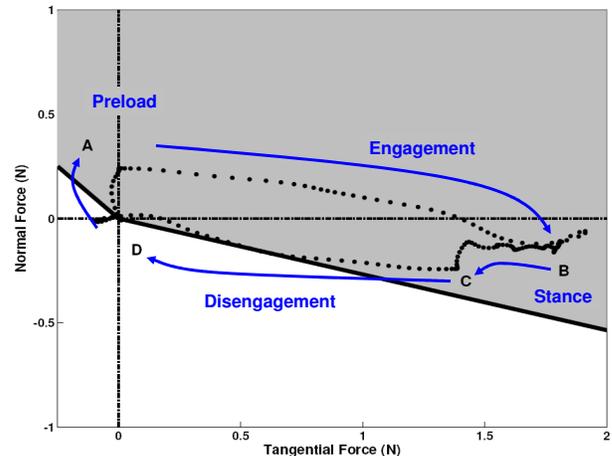

Fig. 11. Tangential and normal contact forces of StickyBot's front left foot during one climbing step. Approximate (from Eq. 2) tangential-normal contact limits for one foot are also shown. Initial normal preload (A) brings DPS patches into contact with the climbing substrate and then increasing tangential force allows the foot to sustain the required adhesive loads (A-B). At the end of stance (B) the right front foot is brought into contact, increasing the adhesive force at the left foot (C). Smooth detachment is achieved by moving the contact force to the origin in force-space and intersecting the limit surface (D).

rear feet controlled for maximum stability (consistent with a maximum tangential force of 3N, established by actuator limits). A few interesting observations emerge from the plot. On a horizontal surface, gravity does not assist in loading the feet in shear and maximum stability is obtained by reversing the rear feet and pulling inward against the front feet in the fore-aft direction. Thus, a gecko on a shaking leaf or branch might want to reverse its rear feet for maximum stability.

For steep slopes, gravity provides most of the tangential loading needed to generate adhesion and best results are obtained with the rear feet aligned with the front feet. This is the mode in which StickyBot normally operates. The tail is particularly helpful on steep slopes to reduce the necessary adhesive force at the front limbs. However, as the surface becomes overhanging and ultimately inverted, the tail is counterproductive and the front and rear feet must pull in opposition to each other to generate adhesion. Although StickyBot is only able to generate ∼3N of sustained tangential force at each foot, by reversing the rear feet it is able to cling to surfaces with an overhang angle of at least 20° as shown in Fig. 1.

The limit surface is also useful in planning force trajectories for the feet during an attachment, loading and detachment cycle. Figure 11 shows the tangential and normal contact forces exerted by StickyBot's front left foot during one climbing step. StickyBot only controls internal forces in the tangential (fore-aft) direction and, because we are climbing vertically, the lateral forces are small. Therefore, only the tangential-normal cross section of the limit surface is shown. Also, when climbing, StickyBot generally does not achieve a full normal preload to obtain maximum adhesion as in Fig. 4. Consequently, we assume that $\alpha^* \approx 15°$, consistent with a light preload.

A nominal force cycle starts with a modest preload (A) to bring the DPS patches into good contact with the climbing substrate. However, the normal force should not be so large that it tends to push the robot off the wall. The shear forces are then increased (A-B) so that the available adhesion also

increases for the stance phase (B). Toward the end of the stance phase, the opposite (right) front foot requires an initial normal preload, which increases the required adhesion at the left foot (C) to maintain equilibrium. When it is time to detach the foot, the shear load and adhesion are simultaneously reduced (C-D) and transferred to the right front foot. Because the limit surface of the DPS intersects the origin, the foot can be released effortlessly and smoothly (D), with little energy expended in detaching it from the surface.

The actual forces for a typical cycle are plotted in Fig. 11 and labeled with respect to the nominal cycle described by (A-D). The only significant differences are due to dynamic effects when the opposite foot is coming into contact (B-C) and at liftoff (D). These differences suggest the value of a dynamic analysis, as discussed in the next section.

V. CONCLUSIONS AND FUTURE WORK

We described a three-dimensional limit surface in contact force space for representing the friction and adhesion limits associated with a synthetic directional adhesive material. The limit surfaces for individual patches are combined and linearized to produce a set of contact constraints for each foot of a climbing robot. The limit surfaces are convex and they intersect the origin in force space. These properties lead to efficient strategies for controlling internal forces between the feet to maximize the margin of stability with respect to disturbances and for attaching and detaching the feet smoothly, without unproductive energy expenditure.

Because the limit surfaces are asymmetric, foot orientation is also important. Observations of geckos reveal that they change the orientations of their feet, for example when

clinging to a ceiling (see Fig. 9) or when running head-first down a wall. An important development for StickyBot then, is to add a degree of freedom at the ankles so that the rear feet, especially, can rotate. An interesting first step could be to make this degree of freedom passive, so that the rear feet are aligned like the casters on a rolling desk chair in response to tangential and lateral forces during the attachment phase, before adhesion prevents further rotation. An active tail will also be useful, both to prevent it from hindering performance on overhanging surfaces and to facilitate transitions from horizontal to vertical surfaces.

The analysis in this paper can also be extended to address dynamic climbing. Already, when climbing at $6\mathrm{cm/s}$ with a stride frequency of $0.5\mathrm{Hz}$, StickyBot generates inertial forces high enough to affect the force balance, as indicated by the disturbances at points (B) and (D) in Fig. 11.

Additional work is underway to develop materials that achieve higher levels of adhesion, especially on surfaces that are not completely smooth, without requiring a high normal preload. This will make the force optimization problem less heavily constrained and may lead to an optimization that seeks to reduce actuator effort while maintaining a consistent margin of stability; a strategy which seems to be pursued in nature.

REFERENCES

[1] Alan T. Asbeck, Sangbae Kim, M. R. Cutkosky, William R. Provancher, and Michele Lanzetta. Scaling hard vertical surfaces with compliant microspine arrays. *Int. J. Rob. Res.*, 25(12):1165–1179, 2006.

[2] K. Autumn. *Biological Adhesives*, volume XVII. Springer-Verlog, Berlin Heidelberg, 2006.

[3] K. Autumn, A. Dittmore, D. Santos, M. Spenko, and M. Cutkosky. Frictional adhesion: a new angle on gecko attachment. *J Exp Biol*, 209(18):3569–3579, 2006.

[4] K. Autumn and A. Peattie. Mechanisms of adhesion in geckos. *Integrative and Comparative Biology*, 42(6):1081–1090, 2002.

[5] K. Autumn, M. Sitti, Y. Liang, A. Peattie, W. Hansen, S. Sponberg, T. Kenny, R. Fearing, J. Israelachvili, and R. Full. Evidence for van der waals adhesion in gecko setae. *Proc. of the National Academy of Sciences of the USA*, 99(19):12252–12256, 2002.

[6] C. Balaguer, A. Gimenez, J. Pastor, V. Padron, and C. Abderrahim. A climbing autonomous robot for inspection applications in 3d complex environments. *Robotica*, 18(3):287–297, 2000.

[7] K. Daltorio, A. Horchler, S. Gorb, R. Ritzmann, and R. Quinn. A small wall-walking robot with compliant, adhesive feet. In *Proc. of the International Conference on Intelligent Robots and Systems*, pages 3648–3653, Alberta, Canada, 2005.

[8] B.V. Derjaguin. *Kolloid Z.*, 69:155, 1934.

[9] D. Dowson. *History of Tribology*. Professional Engineering Publishing Limited, London, 2nd edition, 1998.

[10] A. Goldman and A. Tucker. Polyhedral convex cones. In H. Kuhn and A. Tucker, editors, *Linear Inequalities and Related Systems. Annals of Mathematics Studies 38*, pages 19–39. Princeton University Press, Princeton, NJ, 1956.

[11] S. Hirai and H. Asada. Kinematics and static of manipulation using the theory of polyhedral convex cones. *International Journal of Robotics Research*, 12(5):434–447, 1993.

[12] K.L. Johnson. Adhesion and friction between a smooth elastic spherical asperity and a plane surface. *Proc. of the Royal Society A: Mathematical, Physical and Engineering Sciences*, 453(1956):163–179, 1997.

[13] K.L. Johnson, K. Kendall, and A.D. Roberts. Surface energy and the contact of elastic solids. *Proceedings of the Royal Society of London. Series A, Mathematical and Physical Sciences*, 324(1558):301–313, 1971.

[14] J. Kerr and B. Roth. Analysis of multifingered hands. *The International Journal of Robotics Research*, 4(4):3–17, 1986.

[15] S. Kim, M. Spenko, S. Trujillo, B. Heyneman, V. Matolli, and M. Cutkosky. Whole body adhesion: hierarchical, directional and distributed control of adhesive forces for a climbing robot. In *Proc. of the IEEE International Conference on Robotics and Automation*, pages 1268–1273, Rome, Italy, 2007.

[16] G. La Rosa, M. Messina, G. Muscato, and R. Sinatra. A lowcost lightweight climbing robot for the inspection of vertical surfaces. *Mechatronics*, 12(1):71–96, 2002.

[17] R. Lal Tummala, R. Mukherjee, N. Xi, D. Aslam, H. Dulimarta, J. Xiao, M. Minor, and G. Dang. Development of a tracked climbing robot. *Journal of Intelligent and Robotic Systems*, 9(4), 2002.

[18] M. P. Murphy and M. Sitti. Waalbot: An agile small-scale wall-climbing robot utilizing dry elastomer adhesives. *Mechatronics, IEEE/ASME Transactions on*, 12(3):330–338, 2007.

[19] D. Santos, S. Kim, M. Spenko, A. Parness, and M. Cutkosky. Directional adhesive structures for controlled climbing on smooth vertical surfaces. In *IEEE ICRA*, Rome, Italy, 2007. Accepted.

[20] A. Saunders, D. Goldman, R. Full, and M. Buehler. The rise climbing robot: body and leg design. In *SPIE Unmanned Systems Technology VII*, volume 6230, Orlando, FL, 2006.

[21] J. Savall, A. Avello, and L. Briones. Two compact robots for remote inspection of hazardous areas in nuclear power plants. *Robotics and Automation, 1999. Proceedings. 1999 IEEE International Conference on*, 3:1993–1998 vol.3, 1999.

[22] A.R. Savkoor and G.A.D. Briggs. The effect of tangential force on the contact of elastic solids in adhesion. *Proc. of the Royal Society A: Mathematical, Physical and Engineering Sciences*, 356(1684):103–114, 1977.

[23] Z. Xu and P. Ma. A wall-climbing robot for labeling scale of oil tank's volume. *Robotica*, 20(2):203–207, 2002.

[24] H. Yoshizawa, Y. Chen, and J. Israelachvili. Fundamental mechanisms of interfacial friction. 1. relation between adhesion and friction. *Journal of Physical Chemistry*, 97:4128–4140, 1993.